Mechanism for Explaining Differences in the Order Parameters of FeAs-Based and FeP-Based Pnictide Superconductors

Ronny Thomale, Christian Platt, Werner Hanke, and B. Andrei Bernevig

Phys. Rev. Lett. **106**, 187003 — Published 6 May 2011

DOI: 10.1103/PhysRevLett.106.187003

Why some Iron-based superconductors are nodal while others are nodeless

Ronny Thomale,[1] Christian Platt,[2] Werner Hanke,[2] and B. Andrei Bernevig[1]

[1] *Department of Physics, Princeton University, Princeton, NJ 08544*
[2] *Institute for Theoretical Physics and Astrophysics, University of Würzburg, Am Hubland, D 97074 Würzburg*

We put forward a scenario that naturally explains the difference between the order-parameter character in arsenide (As) and phosphorous (P) iron-based superconductors. Using functional renormalization group techniques to analyze it in detail, we find that nodal superconductivity on the electron pockets (hole pocket gaps are always nodeless) can naturally appear when the hole pocket at (π, π) in the unfolded Brillouin zone is absent, as is the case in LaOFeP. There, electron-electron intra-orbital interactions render the gap on the electron pockets softly nodal (of $s^{\pm}$ form). When the pocket is present, it is of d_{xy} orbital character and the intra-orbital interaction with the d_{xy} dominated part of the electron Fermi surface tends to drive the superconductivity nodeless.

PACS numbers: 74.20.Mn, 74.20.Rp, 74.25.Jb, 74.72.Jb

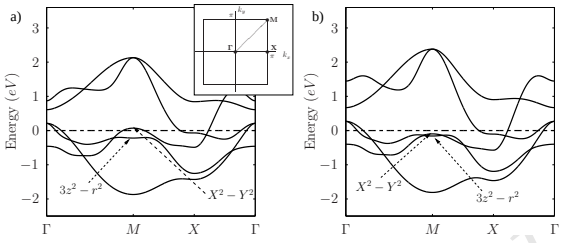

FIG. 1. 2D Band structure for LaOFeAs (a) and LaOFeP (b). (Inset: Brillouin Zone). The tight-binding model for LaOFeAs contains in-plane hoppings up to fifth nearest-neighbors [5]; the parameters are varied for LaOFeP according to the different pnictogen height parameters given in [14]. The dashed horizontal lines denote the Fermi level for the undoped compound. The electronic structure looks very similar in both systems. The major difference is the $d_{X^2-Y^2}$ dominated band crossing the Fermi level in (a), but not in (b).

After two years of intense research in the new iron-based superconductors (pnictides) [1], the symmetry of the order parameter is still far from settled. Theoretically, the current opinion converged on an $s^{\pm}$ order parameter that changes sign between the electron (e) and hole (h) pockets, which comes out of both strong and weak-coupling pictures of the iron-based superconductors originating from inter-pocket pair hopping [2–8]. The method of choice in the intermediately correlated pnictides is likely the functional renormalization group (FRG), which systematically takes into account the competing ordering tendencies in the system [8–13]. Previous FRG work gives anisotropic gaps around the e-pockets which, at their smallest value, are close to but do not cross zero [9]. The experimental situation appears such that in pnictides such as LaOFeAs, a majority of experiments point to the existence of nodeless isotropic gaps [15, 16] on the hole (h) Fermi surface (FS) and also nodeless gaps on the electron (e) FS, albeit with a larger gap-anisotropy [17–22]. In contrast, in LaOFeP, a clear majority of experiments are in favor of a nodal gap behavior on the e-pockets [23, 24]. This difference is even more puzzling, since both materials display similar e- and h-pockets at X- and Γ-points (see Fig. 1) [25].

In this article, we offer an explanation for the difference between the order parameter character in the As and P-based compounds. Using FRG on a 5-band model of the pnictides with orbital interactions, we find that the gap on the e-pockets can undergo a nodal transition if the h-pocket at (π, π) (M) is absent. On the basis of RPA calculations, Kuroki *et al.* [14] already argued that the appearance of the FS around (π, π) in the unfolded BZ is sensitive to the pnictogen height measured from the Fe plane and may drive a nodal or a nodeless pairing. In contrast to the FRG, however, the RPA assumes right from the outset a magnetically driven SDW-type of pairing interaction. In the FRG, one starts from the "bare" many-body interaction (Eq. 2 below) in the Hamiltonian and the pairing is dynamically generated by systematically integrating out the high-energy degrees of freedom including all important fluctuations on equal footing. In the RPA-calculation the competition between nodal $s^{\pm}$-wave and d-wave pairing is rather subtle and the B_{1g} d-wave solution can win over the nodal $s^{\pm}$-wave for the LaFePO system (Fig. 16a of [14]). This is not what experiments reflect and what we find in the FRG: here the $s^{\pm}$-results (even varying them in a rather wide regime) are very robust. We demonstrate below that they can be understood from a general "orthogonality" principle: In the SC state, the SC pair state has to be "orthogonal" to the repulsive part of the interaction, *i.e.*, putting the e-pairs in an anisotropic wave function [26]. Specifically, in the pnictides, the repulsive interaction connects the FS pockets around Γ-, X- and, if present, also M-points. Though repulsive in the singlet channel, the corresponding contributions yield strong pairing provided the gap function on the two sets of FS have opposite sign. We show in this Letter that the generalization of the original $s^{\pm}$-state argument [3, 5] acting between Γ- and X-pockets, is also at work for the cases considered here, and

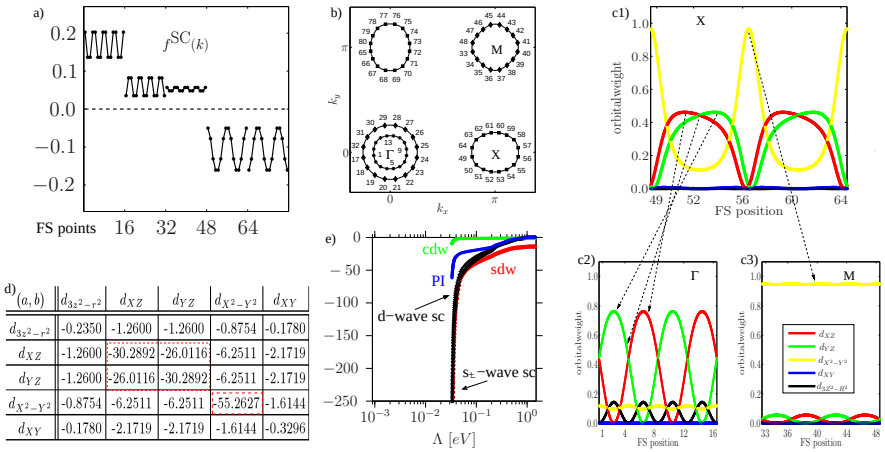

d)

(a,b)	$d_{3z^2-r^2}$	d_{XZ}	d_{YZ}	$d_{X^2-Y^2}$	d_{XY}
$d_{3z^2-r^2}$	-0.2350	-1.2600	-1.2600	-0.8754	-0.1780
d_{XZ}	-1.2600	-30.2892	-26.0116	-6.2511	-2.1719
d_{YZ}	-1.2600	-26.0116	-30.2892	-6.2511	-2.1719
$d_{X^2-Y^2}$	-0.8754	-6.2511	-6.2511	-55.2627	-1.6144
d_{XY}	-0.1780	-2.1719	-2.1719	-1.6144	-0.3296

FIG. 2. (Color online). 5 pocket scenario for LaOFeAs. a) Plot of the SC form factor gap $f^{\mathrm{SC}}(k)$ versus the patching indices (momenta) shown in b). The gap on the outer h-pocket at Γ is smaller than of the inner h-pocket and of the same order as the M pocket gap. The gap on the e-pockets is very anisotropic but nodeless and of opposite sign from h-pocket gap. c1)-c3) Orbital weight distribution on the different pockets (h-pocket at Γ is similar to c2) shifted by 90 degrees). Dashed lines indicate relevant scattering contributions for U_1 interaction. d) Leading orbital-decomposed SC instability eigenvalues $c^{\mathrm{SC}}_{i,(a,b)}(\Lambda_c)$ from (3). $d_{XZ,YZ}$ and $d_{X^2-Y^2}$ scattering dominates. e) Flow of leading instability eigenvalues (charge density wave (CDW), Pomeranchuk instability (PI), SDW, and SC). SDW fluctuations are relevant; the leading instability is $s^{\pm}$-SC at $\Lambda_c \approx 0.03eV$, B_{1g} d-wave SC and SDW diverge in close proximity below (hardly distinguishable on the logarithmic scale).

explains the propensity to a nodal or nodeless SC gap.

We use a two-dimensional tight-binding model [5] to describe the 1111-type pnictides:

$$H_0 = \sum_{\boldsymbol{k},s} \sum_{a,b=1}^{5} c^{\dagger}_{\boldsymbol{k}as} K_{ab}(\boldsymbol{k}) c_{\boldsymbol{k}as}. \qquad (1)$$

Here c's denote electron annihilation operators, a, b the five Fe d-orbitals, and s the spin indices. While the main electronic structure of P-based and As-based compounds is very similar, there are certain important differences. Fig. 1 shows the band structure of LaOFeAs and LaOFeP, where the latter is obtained by adjusting the parameters in [5] according to the changed pnictogen height from As to P [14]. In the vicinity of the Fermi surface, the most notable difference is the presence or absence of a broad $d_{X^2-Y^2}$ (d_{xy})-dominated band at $M = (\pi, \pi)$, in agreement with ARPES data. To account for this difference, we use a 5 *pocket scenario* for the *As-based* and a 4 *pocket scenario* for the *P-based* compounds. We, thus, choose to compare and analyze two generic cases, with or without the h-pocket at M as corresponding to the As-based 1111 (122) and the P-based compounds, respectively.

The interactions in the orbital model are given by:

$$H_{\mathrm{int}} = \sum_i \Bigg[U_1 \sum_a n_{i,a\uparrow} n_{i,a\downarrow} + U_2 \sum_{a<b,s,s'} n_{i,as} n_{i,bs'} + \sum_{a<b} (J_{\mathrm{H}} \sum_{s,s'} c^{\dagger}_{ias} c^{\dagger}_{ibs'} c_{ias'} c_{ibs} + J_{\mathrm{pair}} c^{\dagger}_{ia\uparrow} c^{\dagger}_{ia\downarrow} c_{ib\downarrow} c_{ib\uparrow}) \Bigg], \qquad (2)$$

where $n_{i,as}$ denote density operators at site i of spin s in orbital a. We consider intra- and inter-orbital interactions U_1 and U_2 as well as Hund's coupling J_{H} and pair hopping J_{pair}. In what follows, a physical interaction setting is chosen dominated by intra-orbital coupling, $U_1 > U_2 > J_{\mathrm{H}} \sim J_{\mathrm{pair}}$, taking $U_1 = 3.5eV, U_2 = 2.0eV, J_{\mathrm{H}} = J_{\mathrm{pair}} = 0.7eV$ [9]. In terms of interaction scale ratios, this choice roughly corresponds to interaction parameters obtained by constrained RPA ab initio calculations [27]. Below, we comment on the dependence of the SC form factor on the full parameter space.

Using FRG [9–11, 28, 29], we study how the renormalized interaction described by the 4-point function (4PF) evolves under integrating high energy fermionic modes: $V_\Lambda(\boldsymbol{k}_1, n_1; \boldsymbol{k}_2, n_2; \boldsymbol{k}_3, n_3; \boldsymbol{k}_4, n_4) c^{\dagger}_{\boldsymbol{k}_4 n_4 s} c^{\dagger}_{\boldsymbol{k}_3 n_3 \bar{s}} c_{\boldsymbol{k}_2 n_2 s} c_{\boldsymbol{k}_1 n_1 \bar{s}}$, where the flow parameter is the IR cutoff Λ approaching the Fermi surface, and with $\boldsymbol{k}_1$ to $\boldsymbol{k}_4$ the incoming and outgoing momenta, and n_1 to n_4 the band index. Due to the spin rotational invariance of interactions, we constrain ourselves to the $S^z = 0$ subspace of incoming momenta $\boldsymbol{k}_1, \boldsymbol{k}_2$ (and outgoing $\boldsymbol{k}_3, \boldsymbol{k}_4$) and generate the singlet and triplet channel by symmetrization and antisymmetrization of the 4PF V_Λ [28]. The starting conditions are given by the bandwidth serving as an UV cutoff, with the bare initial interactions for the 4PF. The diverging channels of the 4PF under the flow to the Fermi surface signal the nature of the instability, and the corresponding Λ_c serves as an upper bound for the transition temperature T_c. For a given instability characterized by some order parameter $\hat{O}_{\boldsymbol{k}}$ (the most important example of which is the SC instability $\hat{O}^{\mathrm{SC}}_{\boldsymbol{k}} = c_{\boldsymbol{k}} c_{-\boldsymbol{k}}$ in our case), the 4PF in the particular ordering channel can be written as $\sum_{\boldsymbol{k},\boldsymbol{p}} V_\Lambda(\boldsymbol{k}, \boldsymbol{p}) [\hat{O}^{\dagger}_{\boldsymbol{k}} \hat{O}_{\boldsymbol{p}}]$ [12].

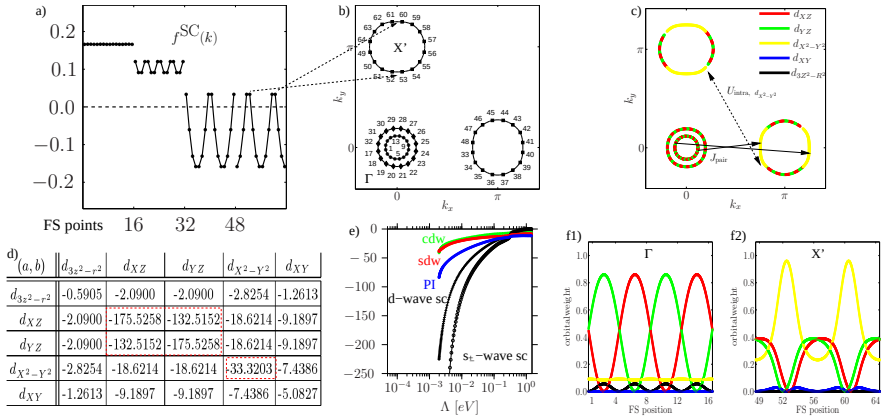

d)(a,b)	$d_{3z^2-r^2}$	d_{XZ}	d_{YZ}	$d_{X^2-Y^2}$	d_{XY}
$d_{3z^2-r^2}$	-0.5905	-2.0900	-2.0900	-2.8254	-1.2613
d_{XZ}	-2.0900	-175.5258	-132.5152	-18.6214	-9.1897
d_{YZ}	-2.0900	-132.5152	-175.5258	-18.6214	-9.1897
$d_{X^2-Y^2}$	-2.8254	-18.6214	-18.6214	-33.3203	-7.4386
d_{XY}	-1.2613	-9.1897	-9.1897	-7.4386	-5.0827

FIG. 3. (Color online). 4 pocket scenario for LaOFeP. a) $s^{\pm}$ SC form factor gap $f^{\mathrm{SC}}(k)$, with FS patches given in b); the $d_{X^2-Y^2}$-dominated h-pocket at M is absent. The h-pockets at Γ are gapped and isotropic, with a smaller gap on the outer h-pocket. The e-pockets show strong anisotropy, being nodal on the pocket tips indicated in Fig. 2b by dashed arrows. c) Pair scattering and, in particular, e-e intra-orbital processes between different e-pockets become important (orbital weights of the pockets are shown in f1)-f2)). d) The orbital decomposition matrix of the SC instability shows a large $d_{XZ,YZ}$ and less relevant $d_{X^2-Y^2}$ contribution. e) Flow of leading instability eigenvalues (notation as in Fig. 2e); nodal $s^{\pm}$ is favored; the SDW is comparably weak. The divergence scale $\Lambda_c \approx 0.002eV$ is smaller than in Fig. 2.

Accordingly, the 4PF in the Cooper channel can be decomposed into different eigenmode contributions $V^{\mathrm{SC}}_{\Lambda}(\boldsymbol{k},-\boldsymbol{k},\boldsymbol{p}) = \sum_i c^{\mathrm{SC}}_i(\Lambda) f^{\mathrm{SC},i}(\boldsymbol{k})^* f^{\mathrm{SC},i}(\boldsymbol{p})$, where i is a symmetry decomposition index ordered such that $i=1$ labels the leading order, i.e. the leading instability of the SC channel corresponds to the eigenvalue $c^{\mathrm{SC}}_1(\Lambda)$ first diverging under the flow of Λ. $f^{\mathrm{SC},i}(\boldsymbol{k})$ is the SC form factor of pairing mode i revealing the SC pairing symmetry and hence gap structure associated with it. In FRG, from the final Cooper channel 4PFs, this quantity is computed along the discretized Fermi surfaces (leading instability form factors are plotted in Fig. 2a and 3a).

As-based compounds: For the As-based setting (Fig. 2), we find that the $s^{\pm}$ *instability, giving rise to different gap signs on h- versus e-pockets, is the leading instability* of the model at moderate doping. The setup resembles the situation studied in [9], which, as an additional check, we also studied with a more detailed tight-binding structure beyond 5th next-nearest neighbors [5]. We also find a nodeless $s^{\pm}$ SC leading instability. In addition, we can identify the *h-pocket at M to play a major role* in contributing to the fully gapped s-wave and to a sign-change from h- to e-pockets (Fig. 2). In particular, we study the orbital content in detail and analyze how the pairing instability distributes over the different orbitals (Fig. 2d). For this, we consider the 4PF in orbital space,

$$V^{\mathrm{orb}}_{c,d\to a,b} = \sum_{n_1,\ldots,n_4=1}^{5} \Big\{ V_{\Lambda}(\boldsymbol{k}_1,n_1;\boldsymbol{k}_2,n_2;\boldsymbol{k}_3,n_3;\boldsymbol{k}_4,n_4) \times u^*_{an_1}(\boldsymbol{k}_1) u^*_{bn_2}(\boldsymbol{k}_2) u_{cn_3}(\boldsymbol{k}_3) u_{dn_4}(\boldsymbol{k}_4) \Big\}, \quad (3)$$

where the u's denote the different orbital components of the band vectors. The matrix shown in Fig. 2d gives the leading eigenvalue contributions of $V^{\mathrm{SC}}_{\Lambda,(a,b)}(\boldsymbol{k},\boldsymbol{p})\; c^{\dagger}_{\boldsymbol{k},a} c^{\dagger}_{-\boldsymbol{k},a} c_{\boldsymbol{p},b} c_{-\boldsymbol{p},b}$, i.e. in the Cooper channel of (3) where constrain ourselves to the dominant processes of Cooper pairs from the same orbital $(a,a) \to (b,b)$. As above, we decompose it into different form factor contributions $\sum_i c^{\mathrm{SC}}_{i,(a,b)}(\Lambda) f^{i,\mathrm{SC}}_{(a,b)}(\boldsymbol{k})^* f^{i,\mathrm{SC}}_{(a,b)}(\boldsymbol{p})$, where the leading eigenvalues at Λ_c for the different (a,b) are given in Fig. 2d and 3d. Intra-orbital scatterings between the d_{xz} (or d_{yz}) orbitals-dominated parts of the e- and Γ h-pockets are most important (Fig. 2). They favor an $s^{\pm}$ SC instability, as was also found in [9]. However, the leading eigenvalue in the As-scenario comes from the diagonal part of the $d_{X^2-Y^2}$ orbital. Pointing in the direction of the $\Gamma \leftrightarrow X$ path, the e-pocket has a high concentration of the $d_{X^2-Y^2}$ orbital. This part of the e-pocket then scatters strongly with the h-pocket at the M-point, which is dominated by the $d_{X^2-Y^2}$ orbital band. The intra-orbital repulsion related to the latter scattering prefers again an $s^{\pm}$-type pairing between the h-pocket at M and the e-pockets, which reinforces the already present $s^{\pm}$ between the Γ h-pockets and the X (X') e-pockets. With the assumption, generally accepted, that U_1 is the dominant interaction, the three h-pockets display a gap of identical sign: the two Γ-pockets which are not nested with each other have the same gap sign, and are of different orbital content than the h-pocket at M. However, the e-pockets contain contributions from all three relevant d orbitals. Therefore, the *e-pockets scatter strongly through U_1 with all three h-pockets*, which enhances the $s^{\pm}$ character of the gap. So, in summary of the As-scenario, the general "orthogonality principle" of having the SC pair state orthogonal to the repulsive interaction induced by the presence of the additional M-pocket further increases the $s^{\pm}$-gap between e- and h-pockets. The h-pocket at M is also responsible for the strong SDW signal (Fig. 2e), as

the nesting wave-vector $M \leftrightarrow X$ is the same as $\Gamma \leftrightarrow X$. Below, for the P-based compounds, we will indeed see that the absence of this pocket weakens the SDW.

P-based compounds: Here, the physical picture changes even qualitatively. As shown in Fig. 3, we find a nodal $s^{\pm}$ scenario for the P-based compounds, with lower critical divergence scale $\Lambda_c \sim T_c$ and less SDW-type fluctuations. The absence of the M h-pocket removes the intra-orbital scattering to the electron pockets. This gives way to previously subleading scattering channels such as, in particular, e-e scattering between the $d_{X^2-Y^2}$-dominated parts of the e-pockets, but also pair hopping from the h-pockets at Γ to the e-pockets. The former acts between the $\boldsymbol{k}$-points of the gap function on the e-pockets given by the peaks and the valleys (red arrow in Fig. 3a) increasing the anisotropy and eventually giving them different signs, thus creating a nodal state, explained again by the "orthogonality requirement".

As another step to substantiate our conclusions, we performed a large sweep in parameter space to resolve the evolution of the SC form factor upon variation of interaction parameters. For the validity of the scenarios above, we find it essential for U_1 to be the leading energy scale. Increasing U_1/U_2 gives better matching with our theory, and we find the condition $U_1/U_2 > 1.3$. Within physically relevant parameters, $U_1/J_{\rm H} > 4$, Hund's coupling does not change the essential structure of the SC form factor. $J_{\rm pair}$ is a sensitive interaction parameter for the P-based compounds. We find that the nodal SC form factor is valid for the parameter regime $U_1/J_{\rm pair} > 4$. Below, the interplay with the e-e scattering, driven by U_1, yields an SC form factor with reduced nodal propensity.

From the ab initio data stated before, we get $U_1/U_2 \approx 1.5$, $U_1/J_{\rm H} = U_1/J_{\rm pair} \approx 6.5$. As such, the parameter regime where the As-based and P-based compounds reside lies in the regime of applicability of our theory. The properties following from there are all consistent with experiment: in the P-based compounds, we find (i) a lower divergence scale and hence lower critical temperature compared to As-based compounds, (ii) significantly enhanced low energy density of states in the (hence nodal) superconducting phase, and (iii) reduced SDW type fluctuations, which, even at pronounced nesting, are insufficient to drive the system to a leading magnetic SDW instability [23–25]. The absence of the hole pocket at M also manifests itself in the orbital decomposition of the pairing instability Fig. 3d: The diagonal contribution of $d_{X^2-Y^2}$, in comparison to $d_{XZ,YZ}$, is reduced. We hence find a correspondence with experiment that applies for the evidence both from SC and SDW ordering.

In summary, we find that the broad band at the unfolded M point plays the major role in explaining the drastic change of SC properties from the As-based to the P-based 1111 compounds, rendering the former nodeless and the latter nodal. The nodes that appear in the P-based compounds are driven by anisotropy of the pair wave function due to the orthogonality requirement of the pair state with respect to the repulsive interactions.

We thank C. Honerkamp, J. Hu, K. Kuroki, D.-H. Lee, D. Scalapino, Z. Tesanovic, A. Vishwanath, and F. Wang for discussions. RT is supported by the Humboldt Foundation and by Sloan Foundation. RT, CP, and WH are supported by DFG-SPP 1458/1, CP and WH by DFG-FOR 538. BAB acknowledges support from the Sloan Foundation and Princeton University startup funds.

Note added. After this work was completed, we became aware of a related independent work studying LaOFeP through FRG [13]. Our data range and interpretation of the numerical results contains and exceeds the case studied there.

[1] Y. Kamihara *et al.*, J. Am. Chem. Soc. **130**, 3296 (2008).
[2] K. Seo, B. A. Bernevig, and J. Hu, Phys. Rev. Lett. **101**, 206404 (2008).
[3] I. I. Mazin *et al.*, Phys. Rev. Lett. **101**, 057003 (2008).
[4] S. Graser *et al.*, New Journal of Physics **11**, 025016 (2009).
[5] K. Kuroki *et al.*, Phys. Rev. Lett. **101**, 087004 (2008).
[6] V. Stanev, J. Kang, and Z. Tesanovic, Phys. Rev. B **78**, 184509 (2008).
[7] M. M. Korshunov and I. Eremin, Phys. Rev. B **78**, 140509 (2008).
[8] A. V. Chubukov, D. V. Efremov, and I. Eremin, Phys. Rev. B **78**, 134512 (2008).
[9] F. Wang *et al.*, Phys. Rev. Lett. **102**, 1047005 (2009).
[10] C. Platt, C. Honerkamp, and W. Hanke, New J. Phys. **11**, 055058 (2009).
[11] R. Thomale *et al.*, Phys. Rev. B **80**, 180505 (2009).
[12] H. Zhai, F. Wang, and D.-H. Lee, Phys. Rev. B **80**, 064517 (2009).
[13] F. Wang, H. Zhai, and D.-H. Lee, Phys. Rev. B **81**, 184512 (2010).
[14] K. Kuroki *et al.*, Phys. Rev. B **79**, 224511 (2009).
[15] L. Wray *et al.*, Phys. Rev. B **78**, 184508 (2008).
[16] H. Ding *et al.*, Eur. Phys. Lett. **83**, 47001 (2008).
[17] K. Matano *et al.*, Eur. Phys. Lett. **83**, 57001 (2008).
[18] M. M. Parish, J. Hu, and B. A. Bernevig, Phys. Rev. B **78**, 144514 (2008).
[19] K. Hashimoto *et al.*, Phys. Rev. Lett. **102**, 207001 (2009).
[20] L. Malone *et al.*, Phys. Rev. B **79**, 140501 (2009).
[21] M. A. Tanatar *et al.*, arXiv:0907.1276.
[22] J. G. Checkelsky *et al.*, arXiv:0811.4668.
[23] M. Yamashita *et al.*, Phys. Rev. B **80**, 220509 (2009).
[24] C. W. Hicks *et al.*, Phys. Rev. Lett. **103**, 127003 (2009).
[25] D. H. Lu *et al.*, Physica C **469**, 452 (2009).
[26] P. W. Anderson, Science **317**, 1705 (2007).
[27] T. Miyake *et al.*, J. Phys. Soc. Jpn. **79**, 044705 (2010).
[28] C. Honerkamp *et al.*, Phys. Rev. B **63**, 035109 (2001).
[29] R. Shankar, Rev. Mod. Phys. **66**, 129 (1994).